ACS APPLIED MATERIALS & INTERFACES

Research Article

www.acsami.org

Dual-Functional WO_3 Nanocolumns with Broadband Antireflective and High-Performance Flexible Electrochromic Properties

Lili Xiao,[†,‡] Ying Lv,[*,†] Wenjie Dong,[†,‡] Nan Zhang,[†] and Xingyuan Liu[*,†]

[†]State Key Laboratory of Luminescence and Applications, Changchun Institute of Optics, Fine Mechanics and Physics, Chinese Academy of Sciences, Changchun 130033, China

[‡]University of Chinese Academy of Sciences, Beijing 100049, China

Supporting Information

ABSTRACT: The three-dimensional, high-porous, and oriented WO_3 nanocolumn film with broadband antireflective and high-performance flexible electrochromic dual-functionalities is achieved by utilizing a simple, one-step, room-temperature glancing angle deposition without any catalysts and templates. It is found that the WO_3 nanocolumn film is effective in increasing the optical transparency in the visible range, enhancing the color-switching response time as well as improving the mechanical flexibility and electrochemical cycling stability in comparison to dense WO_3 film. The further optical, morphological, and electrode reaction kinetics analyses reveal that these improvements can be attributed to its unique porous nanocolumn arrays, which reduce the refractive index, facilitate the interfacial charge-transfer and ion-penetration, and alleviate the internal stress of the film under the bending treatment. These results would provide a simple and effective guidance to design and construct low-cost, robust, flexible, stable, and transparent electrochromic smart windows.

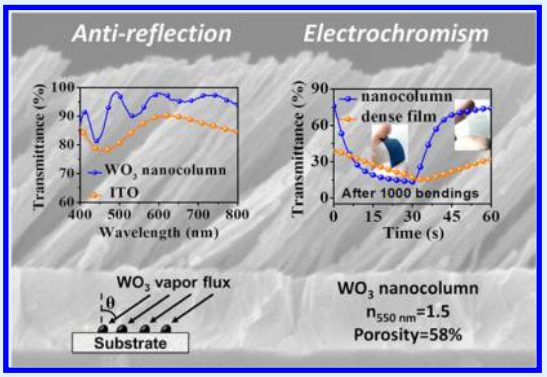

KEYWORDS: *electrochromic, glancing angle deposition, antireflection, flexible, nanostructure, WO_3*

INTRODUCTION

Electrochromic (EC) materials and devices (ECDs) have drawn tremendous attention because of their reversible optical modulation (reflectance, transmittance, and absorption) and exceptional function of vigorously controlled solar energy gain.[1−3] They have found important applications in energy conservation (such as smart windows) together with artificial intelligence (such as displays, antidazzle mirror, and effective disguise). Transition metal oxides such as WO_3, MoO_3, and NiO_x represent the most typical EC materials because of their low cost, simple preparation, high contrast under low driving power, admirable memory effect, and long-lasting stability.[4] However, the inorganic EC materials usually suffer from slow response speed and poor flexibility as compared to organic EC materials, which limits their application in high performance flexible ECDs.[5]

One way to resolve the above problems is in virtue of the construction of nanostructured inorganic EC materials with great specific surface area and permeable channels for fast ion diffusion and electron transfer.[6,7] The unique nanostructure can also help to eliminate the film stress during the bending or twisting treatment, causing a great improvement in mechanical stability and flexibility. Recently, flexible ECDs with enhanced performance have been reported on the basis of the metal-oxides nanomaterials with various morphologies, such as nanoparticles,[8−11] nanowires,[12−14] nanosheets,[15,16] and other interesting configurations[17−20] prepared by sol−gel, hydrothermal, chemical or electrochemical deposition, and other physical deposition methods. Although much progress has been made with the help of nanotechnology, the large-scale and reliable controlled fabrication and integration of nanomaterials with tailorable properties (such as morphology, porosity, and composition) by a convenient method still faces some challenges.[6,7]

Among the various fabrication methods of nanomaterials, glancing angle deposition (GLAD) is considered a versatile vapor-deposition technique, which allows in situ mass production of nanostructured thin film with few material restrictions and lower cost in one step.[21,22] By dynamic varying of the substrate incline and revolution regarding incoming vapor in the GLAD method, the film morphological and physical properties can be precisely adjusted. Moreover, the possibility to work at room temperature makes the GLAD technique more compatible with flexible substrates such as polyethylene terephthalate (PET). Recently, EC properties of nanostructured WO_3,[23−25] MoO_3,[26] and $W_xSi_yO_z$[27,28] films prepared by the GLAD method have been reported, and the relative improvements in EC performance have been observed. Nevertheless, even though the open and polyporous characteristics of these films are very hopeful for their execution as fast

Received: July 19, 2016
Accepted: September 21, 2016
Published: September 21, 2016

DOI: 10.1021/acsami.6b08895
ACS Appl. Mater. Interfaces 2016, 8, 27107−27114

switchable EC layer, as far as we know, high-performance flexible ECDs from GLAD films have not been previously reported. In addition, exhaustive characterization of both their EC and optical performance (especially the antireflective property) is obviously insufficient.

In this study, taking the most studied EC metrical WO_3 as an model, we successfully fabricated a three-dimensional, highly porous, oriented WO_3 nanocolumn on flexible substrate at room temperature by a facile electron-beam evaporation combined GLAD technique. As compared to commonly used GLAD sputtering,[24,27,28] the GLAD electron-beam evaporation system shows better control of the composition, structure, and optical quality of the film due to its lower operating pressure ($<10^{-3}$ Pa) and larger source−substrate distance (make sure the mean free path of the incident vapor is greater than the source−-substrate distance, improving the collimation of incident vapor).[22] We found that the structure, morphology, porosity, and refractive index of WO_3 film can be accurately controlled by simply adjusting the deposition angle in the GLAD method. As compared to the dense bulk WO_3 film, the WO_3 nanocolumn film deposited at an optimized deposition angle of 75° possesses dual antireflective (AR) and EC properties, which not only demonstrated improved optical transmittance in the visible light range but also enhanced EC performance. Most importantly, with the utilization of the dual-functional WO_3 nanocolumns, the highly stable, robust, and flexible ECDs based on GLAD films have been achieved.

EXPERIMENTAL SECTION

Materials. Glass/ITO and PET/ITO substrates were purchased from Shenzhen CSG PV Energy Co. Ltd. Tungsten oxide (WO_3, 99.9%) was purchased from Chnos Elemental Technology Co. Ltd. Propylene carbonate (PC, 99.7%) together with lithium perchlorate ($LiClO_4$, 98%) were acquired from Sigma-Aldrich. All of the chemicals were used without further purification.

Fabrication of Nanostructure WO_3 Films. The nanostructure WO_3 films used in this study were fabricated by the GLAD method using electron beam deposition at room temperature. Ahead of the deposition, the used substrates were cleaned with an ether and ethanol mixture in the ultrasonic apparatus for 10 min, and then dehydrated under hot lamp. The evaporation rate of WO_3 was ∼1.0 nm s^{-1} at pressures of $\sim 2 \times 10^{-3}$ Pa. The film thickness was supervised with a quartz crystal microbalance positioned at the center of chamber; simultaneously the source material was situated at the edge of the vacuum chamber. The deposition angle was modulated from 0° to 75°.

Structural Characterizations. The actual thicknesses of the deposited films were standardized with a surface profiler (XP-1, Ambios, U.S.). The morphological and structural characteristics of the WO_3 films were studied using atomic force microscopy (AFM, SPM-7900, Shimadzu, Japan), scanning electron microscopy (SEM, S-4800, Hitachi, Japan), optical microscopy (BX51TRF, Olympus, Japan), X-ray diffraction (XRD, D8 Focus, Bruker, Germany), and energy dispersive X-ray (EDX, EMAX, Japan) elemental analysis. In EDX analysis, the films were deposited onto Si substrate to eliminate the influence of O element from the ITO substrate. The transmittance and reflectance spectra were obtained using Shimadzu UV-3101PC and PerkinElmer Lambda 1050 UV−vis−NIR spectrophotometers, respectively.

Electrochemical and Electrochromic Evaluation. The electrochemical and EC performances were obtained using a standard three-electrode, one-compartment electrochemical cell. The WO_3 film (18 mm × 18 mm), a titanium sheet (5 mm × 20 mm), and Ag/AgCl (3.5 mol L^{-1} KCl) were utilized as working, assisting, and reference electrodes, respectively. The electrolyte solution was a $LiClO_4$ (1 mol L^{-1}) in PC, which was degassed with nitrogen for 30 min before electrochemical measurements. The transmission spectra of WO_3 films under different potentials were measured by a combination of electrochemical workstation (CHI 920, Shanghai Chenhua, China) and fiber optical spectrometer (QE-Pro, Ocean Optics, U.S.).

RESULTS AND DISCUSSION

Morphological and Structural Characterization. The WO_3 films were deposited by GLAD with various deposition angles (from 0° to 75°, hereafter abbreviated as WO_3-0° to WO_3-75°), which were described as the angle between the WO_3 vapor flux and the normal of substrate. The SEM and AFM measurements indicated an evident change in microstructures and surface morphologies. Figure 1 displays the surface and profile SEMs of the WO_3 films on glass/ITO

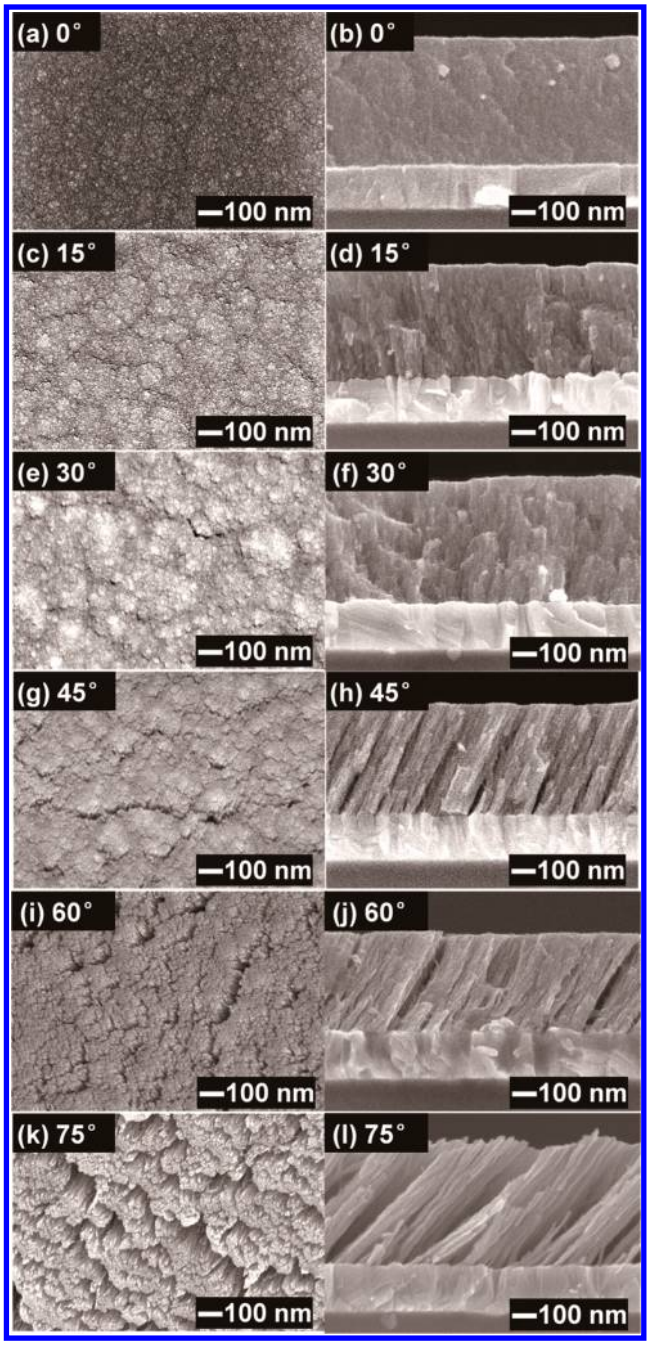

Figure 1. Surface and profile SEMs of WO_3 films on glass/ITO deposited at various angles: (a,b) 0°, (c,d) 15°, (e,f) 30°, (g,h) 45°, (i,j) 60°, and (k,l) 75°.

DOI: 10.1021/acsami.6b08895
ACS Appl. Mater. Interfaces 2016, 8, 27107−27114

deposited for various angles. It can be seen that the WO_3 films prepared at the deposition angle below 30° are continuous, smooth, and compact without pore and crack (Figure 1a–f). However, with the deposition angle increasing from 0° to 30°, some bulky grain agglomeration with the size of ca. 100–200 nm evenly dispersed on the surface, leading to the root-mean-square (RMS) roughness increasing from 2.6 nm for WO_3-0° to 3.7 nm for WO_3-30° (Figure S1). When the deposition angle further increased to 45°, the tilted nanocolumns with nearly compact arrangement were observed (Figure 1g,h). Some pores appear on the surface, and the grain dimension decreases to about 50–100 nm, causing the relatively smooth surface morphologies with the RMS roughness of 3.0 nm. WO_3-60° film displays a nanocolumn structure similar to that of the WO_3-45° film except that the porosity on the WO_3-60° surface increased in some content (Figure 1i,j). With further increasing of deposition angle, the WO_3-75° film reveals oblique, ordered, and disjunctive nanocolumns with the feature size less than 20 nm and the distinct pore with the diameter of about 70 nm (Figure 1k,l). In addition, quite rough, porous, and loose surface features with the RMS roughness of 3.9 nm were clearly detected on the WO_3-75° surface. Therefore, by simply adjusting the deposition angle, the precise regulation of the film porosity and microstructure was successfully achieved in the GLAD method. The unique microstructure for the WO_3-75° film could effectively increase the electrode/electrolyte contact areas and facilitate the charge transfer and ion migration in the electrochemical process.

The microstructures and chemical composition of WO_3 films were also studied by XRD and EDX. Figure 2a displays the

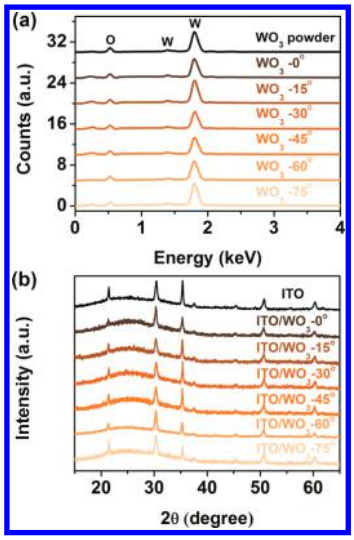

Figure 2. (a) Energy-dispersion X-ray spectra of WO_3 powder and WO_3 films on Si substrate. (b) XRD patterns of ITO, ITO/WO_3 films fabricated at different angles.

EDX spectrum of the deposited WO_3 thin films and the WO_3 powder (raw material). The good agreement in peak positions and intensities as well as the absence of any other peaks except those attributed to W and O from the films and the WO_3 powder strongly suggest that the as-deposited films are nearly stoichiometric (atomic ratio of O/W = 2.96 ± 0.05) without any elemental impurities. XRD analysis indicates the amorphous nature of the deposited WO_3 films, because there was no considerable crystalline peak detected (Figure 2b). A similar result has also been reported in previous studies.[29,30] It has been demonstrated that amorphous WO_3 film generally exhibited EC performance superior to that of crystalline WO_3 film because their toughly chaotic and loose structure facilitates fast ion diffusion and rapid color alteration.[31,32]

Optic Properties. The transmission and reflectance spectra of bare ITO and the WO_3 films deposited at various angles are shown in Figure 3a and Figure S2. As compared to the bare

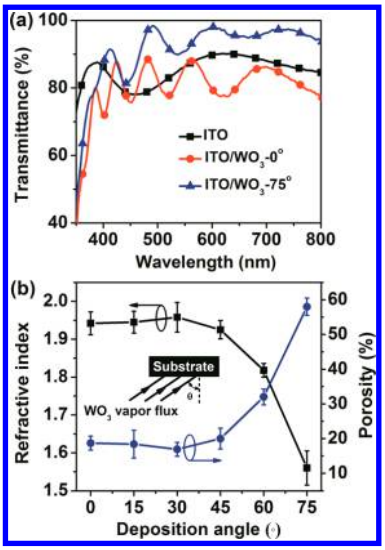

Figure 3. (a) Optical transmittance spectrum of bare ITO and ITO/WO_3 films at normal incidence. (b) Measured refractive index (550 nm) at normal incidence (n_z) and estimated porosity of WO_3 films versus glazing angle in glancing-angle deposition. The error bar indicates the standard deviation of four separate samples.

ITO, the relatively low transmittance of ITO/WO_3-0° film in the visible light range (82.1% vs 85.4%, 400–800 nm) could be mainly attributed to the additional interface reflectance (12.8% vs 11.3%) and absorption of the compact WO_3 film. In contrast, the ITO/WO_3-75° film with nanocolumn structure exhibits an improved optical transmittance to bare ITO. The average optical transmittance of ITO/WO_3-75° film in the visible light range (400–800 nm) was 93.8%, which is enhanced by 8.4% in comparison with 85.4% of bare ITO electrode. In addition, the measured reflectance values in the wavelength of 400–800 nm of bare ITO and ITO/WO_3-75° are 11.3% and 4.9%, respectively (Figure S2). Therefore, the improved transparency could be ascribed to the inherent antireflective capability caused by the WO_3 nanocolumn layer with ultralow refractive index.[33] The sizes of the individual nanocolumn and gaps between them are far smaller than the visible wavelength, suggesting that the Mie and Rayleigh scattering can be ignored and the film can be regarded as a uniform medium with consistent refractive index.[34] As shown in Figure 3b, the measured refractive index of WO_3-75° nanocolumn film at the wavelength of 550 nm (at normal incidence) is only 1.5, significantly lower than those of WO_3-0° film (1.94) and bulk WO_3 material (2.1). As we know, the refractive index of a porous film depends on its porosity, so the porosity of each WO_3 film was also estimated according to the following equation:[35]

$$\text{porosity}\ (\%) = \left(1 - \frac{{n_f}^2 - 1}{{n_b}^2 - 1}\right) \times 100\% \quad (1)$$

where n_f and n_b are the refractive index values of the deposited WO_3 films and dense bulk WO_3 material (n_b = 2.1) at the

DOI: 10.1021/acsami.6b08895
ACS Appl. Mater. Interfaces 2016, 8, 27107–27114

wavelength of 550 nm. From Figure 3b, we noted that the calculated porosity for WO_3 films was nearly constant up to the deposition angle of 30°. However, by further increasing the deposition angle from 45° to 75°, the film porosity was enhanced significantly from 20% (45°) to 58% (75°, Figure 3b). The porosity results are well consistent with the SEM measurements and in reasonable agreement with the optical transparency (Figure S2). Apparently, obvious nanocolumn structure with high porosity will result in a marked decrease in refractive index and a distinct increase in transmittance, making the WO_3 thin films possess AR properties. Conventional AR coatings with quarter-wavelength thickness only work at single wavelength.[36] In contrast, the deposited WO_3-75° nanocolumn film yields broad-band AR characteristics with the average transmittance in the visible region over 93.8% (Figure 3a). Although the absolute decrease of reflectance (from 11.3% to 4.5%) in the nanocolumn WO_3 system is not as significant as reported typical AR coatings, the reflectance of 4.5% is comparable to the results of the literature.[37,38] Most importantly, the achieved transmittance of the ITO/WO_3-75° film is the highest value for WO_3 EC film up to now, to the best of our knowledge (Table S1), which is hospitable to certain particular fields like displays and smart windows. In principle, the broadband 100% transmittance can be achieved in GLAD films by unceasingly turning the refractive index between the substrate and the air to completely eliminate the Fresnel reflection.[34] Further improvements in film transparency are under investigation.

Electrochemical and Electrochromic Performances. To appraise the relationship between the deposition angle and the EC properties of WO_3 films, potential-step chronoamperometry was carried out by simultaneously recording transmittance variation. When the driving voltage was switched between 1.0 and −1.0 V (vs Ag/AgCl) repeatedly, the color of these WO_3 thin films changed reversibly from transparent (bleached state) to sullen blue (colored state). The phenomenon can be associated with the intercalation/deintercalation of electrons and Li^+ ions in accordance with the following reaction:

$$WO_3 + xLi^+ + xe^- \leftrightarrow Li_xWO_3 \quad (2)$$

The transmittance modulations for the WO_3 films at 700 nm and in the wavelength range of 300−1600 nm are given in Figure 4a and Figure S3. It can be seen that all of the WO_3 films except WO_3-75° exhibit ultralarge optical modulation of over 75% at 600−1000 nm and 80−86% at 700 nm (Figure S3), which are comparable to those of the reported nanostructured WO_3 films.[7] The relatively low optical contrast for WO_3-75° film (over 60% at 600−1000 nm and 74% at 700 nm) might be because of the significant diminution in equivalent mass thickness, an evaluation of the effective material for electrochromism, due to the unique porous structure. The equivalent mass thickness could be calculated using $d(1 - \text{porosity})$,[26] where d is the physical thickness (500 nm in this work) of a film. The calculated equivalent mass thickness for WO_3-75° film was only 210 nm, which is about one-half of the rest of the WO_3 films (Figure S4). By properly increasing the thickness of the WO_3-75° film, the optical contrast could be enhanced further. It is also worth noting that the nanostructured WO_3 films not only demonstrate high optical modulations in visible light range, but also in near-infrared region (Figure S3). At the wavelength of 1000 nm, the optical contrast of these WO_3 films ranges from 61% (WO_3-75°) to 78% (WO_3-45°), which are among the best ever reported results for WO_3-based EC films.[7,39]

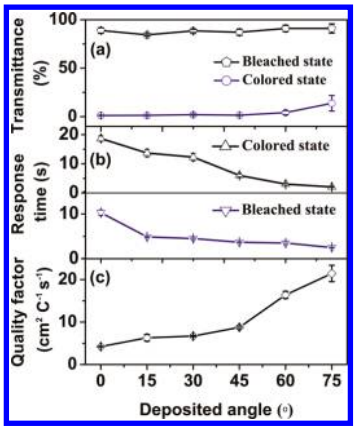

Figure 4. (a) Colored and bleached state transmittance, (b) response time, and (c) quality factor of the WO_3 films deposited at various angles.

The coloration and bleaching response time, time needed for 90% conversion of total optical contrast, of the WO_3 films were also studied at the wavelength of 700 nm. The calculated response time and parallel transmittance changes are given in Figure 4b and Figure S5. As the deposition angle increases from 0° to 75°, the response time of the WO_3 films gradually decreases (Figure 4b). For the WO_3-0° film, the coloration time (τ_c) and bleaching time (τ_b) were 18.6 and 10.3 s, respectively. In contrast, the τ_c and τ_b values for the WO_3-75° film decrease dramatically to 2.1 and 2.5 s under the same conditions, indicating the porous nanocolumn structure can greatly increase the rate of charge transfer and ions intercalation/deintercalation. As compared to many nanostructured WO_3 films, the response time of the reported porous WO_3 nanocolumn in this work is much faster than that of WO_3 nanowires (7.6 and 4.2 s),[40] WO_3 nanorods (272 and 364 s),[41] WO_3 nanosheets (660 and 11 s),[42] and other features (Table S1).

To comprehensively evaluate the overall performance of the EC film, we determined a quality factor $\Gamma_{(\lambda)}$ from the following formulas:[30]

$$\Gamma_{(\lambda)} = \frac{CE_{(\lambda)}}{\tau},\ \tau = \frac{(\tau_c + \tau_b)}{2},\ CE_{(\lambda)} = \frac{\log\left(\frac{T_b}{T_c}\right)}{\Delta Q} \quad (3)$$

where $CE_{(\lambda)}$ is the coloration efficiency, ΔQ is the inserted charge per unit area, and T_b and T_c are the bleached and colored transmittance values, respectively. It was obvious that a greater $\Gamma_{(\lambda)}$ leads to better EC performance. As shown in Figure 4c, the $\Gamma_{(700)}$ of the WO_3 films increases distinctly with the deposition angles increasing. For the WO_3-75° film, the $\Gamma_{(700)}$ value reaches 22.4 $cm^2\ C^{-1}\ s^{-1}$, which is 5 times larger than that of the WO_3-0° film (4.2 $cm^2\ C^{-1}\ s^{-1}$).

The cycling stabilities of the WO_3 films were presented in Figure S6. After 200 successive potential step cycles (±1 V vs Ag/AgCl), both WO_3-0° and WO_3-75° films maintain their transmittance modulation ability with the attenuation of optical contrast for about 7.8% and 8.1%, respectively. The results suggested the good electrochemical durability of the deposited WO_3 films.

Figure 5a illustrates the cyclic voltammetry (CV) trends of these deposited WO_3 thin films. With the increase in deposition

DOI: 10.1021/acsami.6b08895
ACS Appl. Mater. Interfaces 2016, 8, 27107−27114

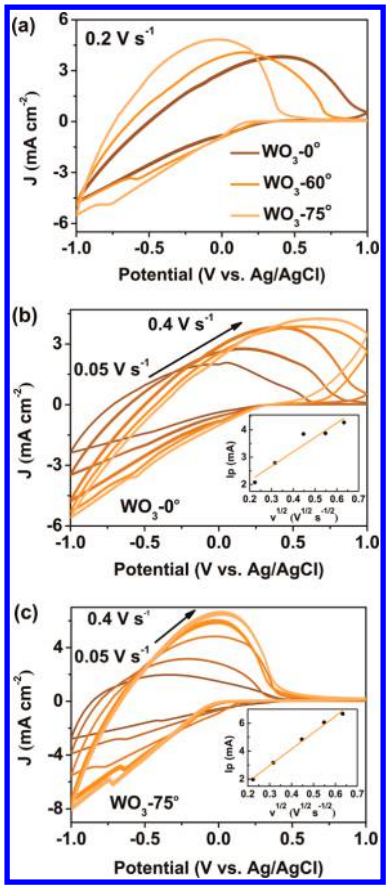

Figure 5. CV curves of (a) WO_3 thin films, (b) WO_3-0°, and (c) WO_3-75° thin films at different scan speeds. The insets give the chart for peak current I_p versus square root of scan speed $v^{1/2}$.

angle, a great increase in area under CV curve and a significant negative-shift of the anodic peak potential were observed, suggesting an enhanced charge capacity and improved redox reversibility of WO_3-75° film. The improvement could be attributed to the porous nanocolumn structures that provide high-active-area and sufficient channels for efficient electrochemical reaction kinetics and fast charge transfer and ions transport.

The diffusion coefficient (D_0) of the Li^+ was determined from CV curves under various scan speed and calculated from the slope of the anodic peak current (I_p) versus the square root of scan speed ($v^{1/2}$, Figure 5b) in accordance with the Randles–Sevcik equation (298 K):[43]

$$I_p = 2.69 \times 10^5 A C_0 D_0^{1/2} n^{3/2} v^{1/2} \quad (4)$$

where A is the area of electrode, C_0 is the electrolyte concentration, and n is the amount of electrons transferred in the reaction (herein, n equals one). The calculated results illustrate that the D_0 in porous WO_3-75° film (1.91×10^{-9} cm^2 s^{-1}) is nearly 5 times that of the compact WO_3-0° film (3.84×10^{-10} cm^2 s^{-1}). Therefore, the increased electrochemical activity and fast ion diffusion of the porous WO_3 nanocolumn film would be the essence of its excellent EC performance.

Flexible Electrochromic Performance. As we know, nanostructured film was one of the most promising candidates for flexible ECDs because of the penetrable channels, large specific surface areas, as well as effective relieving of internal stress. Recently, the high performance flexible EC devices have been obtained by utilizing WO_3 nanosheets[16] or WO_3 nanoparticles[9,12] on flexible ITO or Ag electrode. However, the synthesis and film-formation process of the nanostructured WO_3 are relatively complicated, needing transfer or heat sintering processes. Hereon, we extended our one-step, room-temperature fabricated bifunctional WO_3 nanocolumn film to flexible PET/ITO substrate on which a highly flexible and stable ECD based on GLAD film was achieved.

As shown in Figure 6, the surface features of the flexible WO_3 films are analogous to that of rigid WO_3 films. The flexible WO_3-75° film has distinct nanocolumn structure with the porosity of 49%, causing the high transmittance of 84% and low reflectance of 8.5% at 700 nm (Figure S8), which is among the highest value of reported flexible EC films based on nanostructured WO_3 (Table S2). In contrast, the flexible WO_3-0° film shows a uniform and compact surface feature with the porosity of about 21%, relative low transmittance of 78% at 700 nm, and high reflectance of 16% (Figure S8). Moreover, the calculated D_0 from the CV curves indicated that the flexible WO_3-75° has a more sufficient ion-migration channel than does the WO_3-0° film (Figure S8). So, the excellent structural and electrochemical property of the porous WO_3 nanocolumn was maintained even on the flexible substrate, and the GLAD technique can be used to construct unique nanostructured films for other materials on various substrates.

We further investigated the EC property and bending stability of flexible WO_3 films. As can been seen from Figure 7 and Table S3, the optical contrast, response time, and CE initial state are nearly identical, and the the two flexible WO_3 films on the $\Gamma_{(700)}$ of flexible WO_3-75° (10.1 cm^2 C^{-1} s^{-1}) are a little larger than those on the WO_3-0° film (7.61 cm^2 C^{-1} s^{-1}). Nevertheless, a distinct difference in EC performance was observed after successive bending treatment at a 5 mm radius of curvature. After 500 bending cycles, the optical contrast of WO_3-0° film significantly reduces by 50% (from 79.9% to 38.5%), and the transmittance cannot reach saturate even in 30 s (τ_c = 21.7 s, τ_b = 26.7 s calculated according to the condition

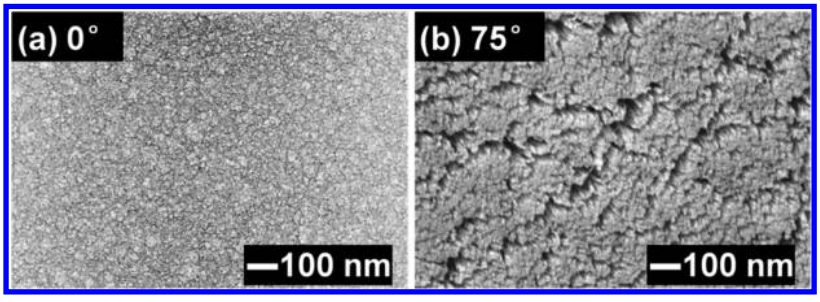

Figure 6. Surface SEM images of flexible (a) WO_3-0° and (b) WO_3-75° thin films on PET/ITO.

DOI: 10.1021/acsami.6b08895
ACS Appl. Mater. Interfaces 2016, 8, 27107–27114

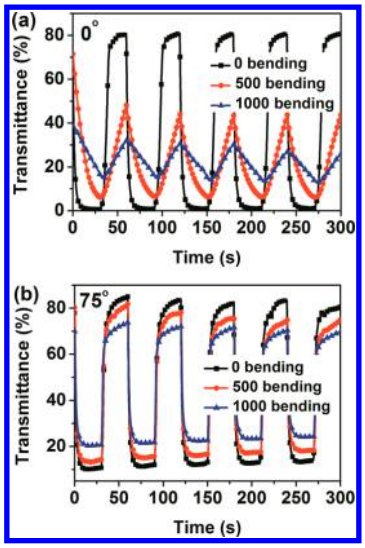

Figure 7. In situ transmittance modulation at 700 nm of flexible (a) WO_3-0° and (b) WO_3-75° thin films on PET/ITO before and after repeated bending at a 5 mm radius of curvature. The potential is switched between 1.0 and −1.0 V (vs Ag/AgCl) at 30 s intervals.

in 30 s), leading to the $\Gamma_{(700)}$ dramatically reduced by 83% (from 7.61 to 1.28 $cm^2\ C^{-1}\ s^{-1}$). By contrast, the optical contrast and $\Gamma_{(700)}$ of WO_3-75° only decreased by 22% (from 73.3% to 57.0%) and 9.3% (from 10.1 to 9.16 $cm^2\ C^{-1}\ s^{-1}$), respectively. Even after 1000 bending cycles, the WO_3-75° films also maintained good EC performance with the optical contrast of 49.8%, response time of τ_c = 4.2 s, τ_b = 7.8 s, and $\Gamma_{(700)}$ of 10.9 $cm^2\ C^{-1}\ s^{-1}$, while the WO_3-0° film presents a lamentable EC performance with the contrast of only 15.2% and $\Gamma_{(700)}$ of 0.9 $cm^2\ C^{-1}\ s^{-1}$.

Figure 8 shows the optical microscope images of these two flexible WO_3 films before and after 1000 repetitive bending

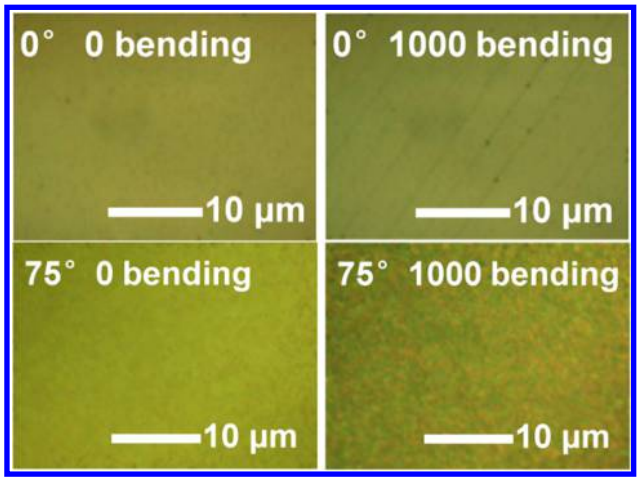

Figure 8. Optical microscope images of flexible WO_3-0° and WO_3-75° thin films on PET/ITO before and after repetitive bending treatment with a 5 mm radius of curvature.

treatment. The surface feature of nanostructured WO_3-75° film remains almost unchanged after bending. By comparison, abundant cracks appear on the WO_3-0° film surface, indicating that the nanostructured WO_3 films exhibit excellent flexibility and advanced mechanical stability, and the nanostructured WO_3 films might be a hopeful candidate for high-performance flexible ECDs.

CONCLUSIONS

The flexible WO_3 nanocolumn films with both broadband AR and outstanding EC properties were achieved by a convenient, one-step GLAD method at room temperature. The WO_3 nanocolumns possess higher transparency of 93.8% and lower reflectance of 4.5% in the visible light range (400−800 nm), higher color-switching speed (τ_c = 2.1 s, τ_b = 2.5 s), and more flexible features (1000 bending cycles) as compared to those of the dense WO_3 film. The primary causes of these improvements lie in their intrinsic low refractive index (n_z = 1.5) for improved antireflection property, high porosity (58%), as well as large active specific surface area for diminishing internal stress and enhancing the interfacial reaction kinetics (D_0 = 1.91 × 10^{-9} $cm^2\ s^{-1}$). The excellent EC performance, perfect AR property, combined with superior flexibility make our GLAD WO_3 nanocolumn-based device a potential candidate in low-cost, high-performance flexible and transparent smart windows. The design and one-step fabrication of a functional film with both AR and EC properties may also provide an interesting twist on the traditional ECD structure, which usually needs extra AR coating (greatly increasing the fabrication cost of ECDs) to improve the transparency and optical manifestation of EC smart windows.

ASSOCIATED CONTENT

Supporting Information

The Supporting Information is available free of charge on the ACS Publications website at DOI: 10.1021/acsami.6b08895.

AFM images; initial transmittance and reflectance spectra; optical contrast and colored/bleached-state transmittance; calculated equivalent mass thickness; in situ transmittance and chronocoulometry switching curve; electrochemical cycling stability, CV curves; transmittance and reflectance spectra of flexible EC films; summary table of flexible EC performance; and summary of reported nanostructured WO_3-based ECDs (PDF)

AUTHOR INFORMATION

Corresponding Authors

*E-mail: lvying@ciomp.ac.cn.
*E-mail: liuxy@ciomp.ac.cn.

Notes

The authors declare no competing financial interest.

ACKNOWLEDGMENTS

We acknowledge financial support from the CAS Innovation Program, National Science Foundation of China (51503196, 61106057, 6140031354), Jilin Province Science and Technology Research Project (20160520176JH, 20140520119JH, 20150101039JC and 20160520092JH), and project supported by State Key Laboratory of Luminescence and Applications.

REFERENCES

(1) Granqvist, C. G. *Handbook of Inorganic Electrochromic Materials*; Elsevier: Amsterdam, 1995.
(2) Mortimer, R. J.; Rosseinsky, D. R.; Monk, P. M. *Electrochromic Materials and Devices*; John Wiley & Sons: New York, 2015.

DOI: 10.1021/acsami.6b08895
ACS Appl. Mater. Interfaces 2016, 8, 27107−27114

(3) Llordes, A.; Garcia, G.; Gazquez, J.; Milliron, D. J. Tunable near-Infrared and Visible-Light Transmittance in Nanocrystal-in-Glass Composites. *Nature* **2013**, *500*, 323−326.
(4) Monk, P. M.; Mortimer, R. J.; Rosseinsky, D. R. *Electrochromism: Fundamentals and Applications*; John Wiley & Sons: New York, 2008.
(5) Mortimer, R. J. Electrochromic Materials. *Annu. Rev. Mater. Res.* **2011**, *41*, 241−268.
(6) Wang, J. M.; Sun, X. W.; Jiao, Z. Application of Nanostructures in Electrochromic Materials and Devices: Recent Progress. *Materials* **2010**, *3*, 5029−5053.
(7) Zheng, H.; Ou, J. Z.; Strano, M. S.; Kaner, R. B.; Mitchell, A.; Kalantar-zadeh, K. Nanostructured Tungsten Oxide − Properties, Synthesis, and Applications. *Adv. Funct. Mater.* **2011**, *21*, 2175−2196.
(8) Costa, C.; Pinheiro, C.; Henriques, I.; Laia, C. A. T. Electrochromic Properties of Inkjet Printed Vanadium Oxide Gel on Flexible Polyethylene Terephthalate/Indium Tin Oxide Electrodes. *ACS Appl. Mater. Interfaces* **2012**, *4*, 5266−5275.
(9) Layani, M.; Darmawan, P.; Foo, W. L.; Liu, L.; Kamyshny, A.; Mandler, D.; Magdassi, S.; Lee, P. S. Nanostructured Electrochromic Films by Inkjet Printing on Large Area and Flexible Transparent Silver Electrodes. *Nanoscale* **2014**, *6*, 4572−4576.
(10) Malavé Osuna, R.; Hernández, V.; López Navarrete, J. T.; Kauppinen, E. I.; Ruiz, V. Ultrafast and High-Contrast Electrochromism on Bendable Transparent Carbon Nanotube Electrodes. *J. Phys. Chem. Lett.* **2010**, *1*, 1367−1371.
(11) Chiang, K.-K.; Wu, J.-J. Fuel-Assisted Solution Route to Nanostructured Nickel Oxide Films for Electrochromic Device Application. *ACS Appl. Mater. Interfaces* **2013**, *5*, 6502−6507.
(12) Costa, C.; Pinheiro, C.; Henriques, I.; Laia, C. A. T. Inkjet Printing of Sol−Gel Synthesized Hydrated Tungsten Oxide Nanoparticles for Flexible Electrochromic Devices. *ACS Appl. Mater. Interfaces* **2012**, *4*, 1330−1340.
(13) Li, K.; Zhang, Q.; Wang, H.; Li, Y. Lightweight, Highly Bendable and Foldable Electrochromic Films Based on All-Solution-Processed Bilayer Nanowire Networks. *J. Mater. Chem. C* **2016**, *4*, 5849−5857.
(14) Yan, C.; Kang, W.; Wang, J.; Cui, M.; Wang, X.; Foo, C. Y.; Chee, K. J.; Lee, P. S. Stretchable and Wearable Electrochromic Devices. *ACS Nano* **2014**, *8*, 316−322.
(15) Grote, F.; Yu, Z.-Y.; Wang, J.-L.; Yu, S.-H.; Lei, Y. Self-Stacked Reduced Graphene Oxide Nanosheets Coated with Cobalt−Nickel Hydroxide by One-Step Electrochemical Deposition toward Flexible Electrochromic Supercapacitors. *Small* **2015**, *11*, 4666−4672.
(16) Liang, L.; Zhang, J.; Zhou, Y.; Xie, J.; Zhang, X.; Guan, M.; Pan, B.; Xie, Y. High-Performance Flexible Electrochromic Device Based on Facile Semiconductor-to-Metal Transition Realized by $WO_3{\cdot}2H_2O$ Ultrathin Nanosheets. *Sci. Rep.* **2013**, *3*, 1936.
(17) Li, H.; Vienneau, G.; Jones, M.; Subramanian, B.; Robichaud, J.; Djaoued, Y. Crack-Free 2D-Inverse Opal Anatase TiO_2 Films on Rigid and Flexible Transparent Conducting Substrates: Low Temperature Large Area Fabrication and Electrochromic Properties. *J. Mater. Chem. C* **2014**, *2*, 7804−7810.
(18) Lin, Y. S.; Chuang, P. Y.; Shie, P. S. Lithium Electrochromic Performance of Flexible Ni Oxide Films Enhanced by Fe Oxide Addition with an Atmospheric Pressure Plasma Jet for Flexible Electrochromic Application. *J. Solid State Electrochem.* **2015**, *19*, 1671−1683.
(19) Lin, Y. S.; Tsai, T. H.; Lu, W. H.; Shie, B. S. Lithium Electrochromic Properties of Atmospheric Pressure Plasma Jet-Synthesized Tungsten/Molybdenum-Mixed Oxide Films for Flexible Electrochromic Device. *Ionics* **2014**, *20*, 1163−1174.
(20) Lin, Y.-S.; Tsai, T.-H.; Hung, S.-C.; Tien, S.-W. Enhanced Lithium Electrochromism of Atmospheric Pressure Plasma Jet-Synthesized Tungsten/Molybdenum Oxide Films for Flexible Electrochromic Devices. *J. Solid State Electrochem.* **2013**, *17*, 1077−1088.
(21) Barranco, A.; Borras, A.; Gonzalez-Elipe, A. R.; Palmero, A. Perspectives on Oblique Angle Deposition of Thin Films: From Fundamentals to Devices. *Prog. Mater. Sci.* **2016**, *76*, 59−153.
(22) Martin, P. M. In *Handbook of Deposition Technologies for Films and Coatings*; Taschuk, M. T., Hawkeye, M. M., Brett, M. J., Eds.; William Andrew Publishing: Boston, 2010; Chapter 13, pp 621−678.
(23) Beydaghyan, G.; Bader, G.; Ashrit, P. V. Electrochromic and Morphological Investigation of Dry-Lithiated Nanostructured Tungsten Trioxide Thin Films. *Thin Solid Films* **2008**, *516*, 1646−1650.
(24) Deniz, D.; Frankel, D. J.; Lad, R. J. Nanostructured Tungsten and Tungsten Trioxide Films Prepared by Glancing Angle Deposition. *Thin Solid Films* **2010**, *518*, 4095−4099.
(25) Chananonnawathorn, C.; Horprathum, M.; Eiamchai, P.; Srichaiyaperk, T.; Aiempanakit, K.; Chindaudom, P. Investigation of Electrochromic WO_3 Nanorods Prepared by DC Reactive Magnetron Sputtering with Glad Technique. In *Applied Physics and Material Applications*; Kaewkhao, J., Limsuwan, P., Kim, H. J., Djamal, M., Eds.; Trans Tech Publications Ltd.: Stafa-Zurich, 2013; pp 136−139.
(26) Beydaghyan, G.; Boudreau, M.; Ashrit, P. V. Optical Properties and Electrochromic Response of Nanostructured Molybdenum Trioxide Films. *J. Mater. Res.* **2011**, *26*, 55−61.
(27) Garcia-Garcia, F. J.; Gil-Rostra, J.; Yubero, F.; Espinós, J. P.; Gonzalez-Elipe, A. R.; Chaboy, J. In Operando" X-Ray Absorption Spectroscopy Analysis of Structural Changes During Electrochemical Cycling of WO_3 and $W_xSi_yO_z$ Amorphous Electrochromic Thin Film Cathodes. *J. Phys. Chem. C* **2015**, *119*, 644−652.
(28) Gil-Rostra, J.; Cano, M.; Pedrosa, J. M.; Ferrer, F. J.; García-García, F.; Yubero, F.; González-Elipe, A. R. Electrochromic Behavior of $W_xSi_yO_z$ Thin Films Prepared by Reactive Magnetron Sputtering at Normal and Glancing Angles. *ACS Appl. Mater. Interfaces* **2012**, *4*, 628−638.
(29) Liu, Y.; Lv, Y.; Tang, Z.; He, L.; Liu, X. Highly Stable and Flexible ITO-Free Electrochromic Films with Bi-Functional Stacked $MoO_3/Ag/MoO_3$ Structures. *Electrochim. Acta* **2016**, *189*, 184−189.
(30) Li, H.; Lv, Y.; Zhang, X.; Wang, X.; Liu, X. High-Performance ITO-Free Electrochromic Films Based on Bi-Functional Stacked $WO_3/Ag/WO_3$ Structures. *Sol. Energy Mater. Sol. Cells* **2015**, *136*, 86−91.
(31) Yang, Y. A.; Cao, Y. W.; Loo, B. H.; Yao, J. N. Microstructures of Electrochromic MoO_3 Thin Films Colored by Injection of Different Cations. *J. Phys. Chem. B* **1998**, *102*, 9392−9396.
(32) Laurenti, M.; Bianco, S.; Castellino, M.; Garino, N.; Virga, A.; Pirri, C. F.; Mandracci, P. Toward Plastic Smart Windows: Optimization of Indium Tin Oxide Electrodes for the Synthesis of Electrochromic Devices on Polycarbonate Substrates. *ACS Appl. Mater. Interfaces* **2016**, *8*, 8032−8042.
(33) Chen, J.-Z.; Ko, W.-Y.; Yen, Y.-C.; Chen, P.-H.; Lin, K.-J. Hydrothermally Processed TiO_2 Nanowire Electrodes with Antireflective and Electrochromic Properties. *ACS Nano* **2012**, *6*, 6633−6639.
(34) Kim, J. K.; Chhajed, S.; Schubert, M. F.; Schubert, E. F.; Fischer, A. J.; Crawford, M. H.; Cho, J.; Kim, H.; Sone, C. Light-Extraction Enhancement of Gainn Light-Emitting Diodes by Graded-Refractive-Index Indium Tin Oxide Anti-Reflection Contact. *Adv. Mater.* **2008**, *20*, 801−804.
(35) Yoldas, B. E. Investigations of Porous Oxides as an Antireflective Coating for Glass Surfaces. *Appl. Opt.* **1980**, *19*, 1425−1429.
(36) Prevo, B. G.; Hwang, Y.; Velev, O. D. Convective Assembly of Antireflective Silica Coatings with Controlled Thickness and Refractive Index. *Chem. Mater.* **2005**, *17*, 3642−3651.
(37) Zheng, B.; Wang, W.; Jiang, G.; Mei, X. Fabrication of Broadband Antireflective Black Metal Surfaces with Ultra-Light-Trapping Structures by Picosecond Laser Texturing and Chemical Fluorination. *Appl. Phys. B: Lasers Opt.* **2016**, *122*, 1−15.
(38) Rahman, A.; Ashraf, A.; Xin, H.; Tong, X.; Sutter, P.; Eisaman, M. D.; Black, C. T. Sub-50-nm Self-Assembled Nanotextures for Enhanced Broadband Antireflection in Silicon Solar Cells. *Nat. Commun.* **2015**, *6*, 5963.
(39) Ma, D.; Shi, G.; Wang, H.; Zhang, Q.; Li, Y. Morphology-Tailored Synthesis of Vertically Aligned 1DWO_3 Nano-Structure Films for Highly Enhanced Electrochromic Performance. *J. Mater. Chem. A* **2013**, *1*, 684−691.

DOI: 10.1021/acsami.6b08895
ACS Appl. Mater. Interfaces 2016, 8, 27107−27114

(40) Zhang, J.; Tu, J.-p.; Xia, X.-h.; Wang, X.-l.; Gu, C. -d., Hydrothermally Synthesized WO_3 Nanowire Arrays with Highly Improved Electrochromic Performance. *J. Mater. Chem.* **2011**, *21*, 5492−5498.
(41) Wang, J.; Khoo, E.; Lee, P. S.; Ma, J. Synthesis, Assembly, and Electrochromic Properties of Uniform Crystalline WO_3 Nanorods. *J. Phys. Chem. C* **2008**, *112*, 14306−14312.
(42) Wang, K.; Zeng, P.; Zhai, J.; Liu, Q. Electrochromic Films with a Stacked Structure of WO_3 Nanosheets. *Electrochem. Commun.* **2013**, *26*, 5−9.
(43) LRFAJ, B. *Electrochemical Methods: Fundamentals and Applications*; Wiley: New York, 2001.

DOI: 10.1021/acsami.6b08895
ACS Appl. Mater. Interfaces 2016, 8, 27107−27114